

Corotational Damping of Diskoseismic C-modes in Black Hole Accretion Discs

David Tsang^{1,2*} and Dong Lai^{1*}

¹*Department of Astronomy, Cornell University, Ithaca, NY 14853, USA*

²*Department of Physics, Cornell University, Ithaca, NY 14853, USA*

14 June 2019

ABSTRACT

Diskoseismic c-modes in accretion discs have been invoked to explain low-frequency variabilities observed in black-hole X-ray binaries. These modes are trapped in the inner-most region of the disc and have frequencies much lower than the rotation frequency at the disc inner radius. We show that because the trapped waves can tunnel through the evanescent barrier to the corotational wave zone, the c-modes are damped due to wave absorption at the corotation resonance. We calculate the corotational damping rates of various c-modes using the WKB approximation. The damping rate varies widely depending on the mode frequency, the black hole spin parameter and the disc sound speed, and is generally much less than 10% of the mode frequency. A sufficiently strong excitation mechanism is needed to overcome this corotational damping and make the mode observable.

Key words: accretion, accretion discs – hydrodynamics – waves – black hole physics – X-rays: binaries

1 INTRODUCTION

Diskoseismic oscillations of accretion discs around relativistic objects have been studied for over two decades (e.g., Kato & Fukue 1980; Okazaki et al. 1987; Nowak & Wagoner 1991, see Wagoner 1999, Kato 2001 for reviews), and have been used as models for the time variability and quasi-periodic oscillations (QPOs) in X-ray emissions from black-hole X-ray binaries.

The c-modes (or so-called corrugation waves) were first proposed to explain low-frequency variabilities as their oscillation frequencies are lower than the associated g-modes and p-modes (see section 3). Kato (1983) and Okazaki & Kato (1985) showed the existence of one-armed ($m = 1$), low-frequency modes in nearly Keplerian (Newtonian) discs, while later work (Kato 1989; Silbergleit et al. 2001) demonstrated the presence of low-frequency c-modes in relativistic accretion discs, particularly the one-armed corrugation waves with a single node ($n = 1$; see section 3 below) in the vertical direction, which oscillate at (approximately) the Lens-Thirring precession frequency evaluated at the outer edge of the trapping region.

In a recent paper (Lai & Tsang 2008), we studied the global corotational instability of non-axisymmetric p-modes ($n = 0$) in black hole accretion discs. The mode is trapped inside the corotation resonance radius r_c (where the wave pattern rotation speed ω/m equals the disc rotation rate Ω) and carries a negative energy. We showed that when the mode frequency ω is sufficiently high, positive wave energy is absorbed at the corotation resonance, leading to the growth of mode amplitude. The mode growth is further enhanced by wave transmission beyond the corotation barrier. Non-axisymmetric g-modes, on the other hand, may contain a corotation resonance in the wave zone. Kato (2003) and Li, Goodman & Narayan (2003) showed that such g-modes are heavily damped as the wave propagate through the corotation resonance (see also Zhang & Lai 2006).

Diskoseismic c-modes are trapped in the inner most regions of black hole accretion discs. Although their primary wave zones are separated from the corotation resonance, the wave can tunnel through the evanescent barrier and propagate again around the corotation. In this paper we calculate the analytic damping rate of c-modes due to wave absorption at the corotation resonance. In section 2 we briefly review the basic properties of perturbations in a thin isothermal disc, and present the basic

* Email: dtsang@astro.cornell.edu; dong@astro.cornell.edu

working perturbation equations. In section 3 we discuss the propagation regions associated with various diskoseismic modes, while in section 4 we demonstrate the effect of the corotation resonance on wave propagation. In section 5 the effect of the corotation on the c-mode is studied and the c-mode damping rates are calculated for different disc parameters. Section 6 contains our conclusion.

2 BASIC SETUP AND EQUATIONS

Consider a thin isothermal disc with the unperturbed velocity $\mathbf{u}_o = (0, r\Omega, 0)$ in the cylindrical coordinates. The vertical density profile is given by (for small $z \ll r$)

$$\rho_o(r, z) = \frac{\Sigma(r)}{\sqrt{2\pi}H} \exp(-z^2/2H^2). \quad (1)$$

Here $\Sigma(r)$ is the (vertically integrated) surface density and $H = c_s/\Omega_\perp$ is the vertical scale height, where Ω_\perp is the vertical oscillation frequency and c_s is the isothermal sound.

Perturbing the mass and momentum conservation equations gives

$$\frac{\partial}{\partial t} \delta\rho + \nabla \cdot (\rho_o \delta\mathbf{u} + \mathbf{u}_o \delta\rho) = 0, \quad (2)$$

$$\frac{\partial}{\partial t} \delta\mathbf{u} + (\mathbf{u}_o \cdot \nabla) \delta\mathbf{u} + (\delta\mathbf{u} \cdot \nabla) \mathbf{u}_o = -\nabla \delta h, \quad (3)$$

with the enthalpy perturbation $\delta h \equiv \delta P/\rho = c_s^2 \delta\rho/\rho$, where we assume that the perturbations are also isothermal. Assuming perturbations of the form $\delta P, \delta\mathbf{u}, \delta\rho \propto \exp(im\phi - i\omega t)$, we have

$$-i\tilde{\omega} \frac{\rho_o}{c_s^2} \delta h + \frac{1}{r} \frac{\partial}{\partial r} (r \rho_o \delta u_r) + \frac{im}{r} \rho_o \delta u_\phi + \frac{\partial}{\partial z} (\rho \delta u_z) = 0 \quad (4)$$

$$-i\tilde{\omega} \delta u_r - 2\Omega \delta u_\phi = -\frac{\partial}{\partial r} \delta h \quad (5)$$

$$-i\tilde{\omega} \delta u_\phi + \frac{\kappa^2}{2\Omega} \delta u_r = -\frac{im}{r} \delta h \quad (6)$$

$$-i\tilde{\omega} \delta u_z = -\frac{\partial}{\partial z} \delta h \quad (7)$$

where $\tilde{\omega} = \omega - m\Omega$. Following Okazaki et al. (1987), we assume a z -dependence of the perturbations such that $\delta h, \delta u_r, \delta u_\phi \propto H_n(z/H)$ where $H_n(Z = z/H)$ is the Hermite polynomial of order n . Then equation (4) reduces to

$$-i\tilde{\omega} \frac{\rho_o}{c_s^2} \delta h + \frac{1}{r} \frac{\partial}{\partial r} (r \rho_o \delta u_r) + \frac{im}{r} \rho_o \delta u_\phi - \frac{n\rho_o}{i\tilde{\omega}} \delta h = 0 \quad (8)$$

Neglecting terms proportional to $dH/dr \sim O(1/r)$, and eliminating the velocity perturbations δu_r and δu_ϕ from equations (5), (6) and (8), we obtain (see eq. [29] in Zhang & Lai [2006])

$$\frac{d^2}{dr^2} \delta h - \left(\frac{d}{dr} \ln \frac{D}{r\Sigma} \right) \frac{d}{dr} \delta h + \left[\frac{2m\Omega}{r\tilde{\omega}} \frac{d}{dr} \ln \frac{D}{\Omega\Sigma} - \frac{m^2}{r^2} - \frac{D(\tilde{\omega}^2 - n\Omega_\perp^2)}{c_s^2 \tilde{\omega}^2} \right] \delta h = 0, \quad (9)$$

where $D = \kappa^2 - \tilde{\omega}^2$. This is our basic working equation.

The approach above is Newtonian. More rigorous fully relativistic derivations of the dispersion relation have been given by Ipser (1994, 1996), Perez et al. (1997), and Silbergleit et al. (2001). Some aspects of the general relativistic effects can be incorporated into our analysis by using the Paczynski-Witta pseudo-Newtonian potential, which gives $\kappa < \Omega = \Omega_\perp$. For our purposes of estimating the c-mode damping rates, it suffices to employ equation (9) but with the relevant fully general relativistic frequencies (e.g., Aliev & Gal'tsov 1981; Okazaki et al. 1987)

$$\Omega = \frac{1}{r^{3/2} + a}, \quad (10)$$

$$\Omega_\perp = \Omega \left(1 - \frac{4a}{r^{3/2}} + \frac{3a^2}{r^2} \right)^{1/2}, \quad (11)$$

$$\kappa = \Omega \left(1 - \frac{6}{r} + \frac{8a}{r^{3/2}} - \frac{3a^2}{r^2} \right)^{1/2}, \quad (12)$$

where the frequencies are in units of c^3/GM , r in units of GM/c^2 , and $a = J_s/M$ is the spin parameter of the black hole.

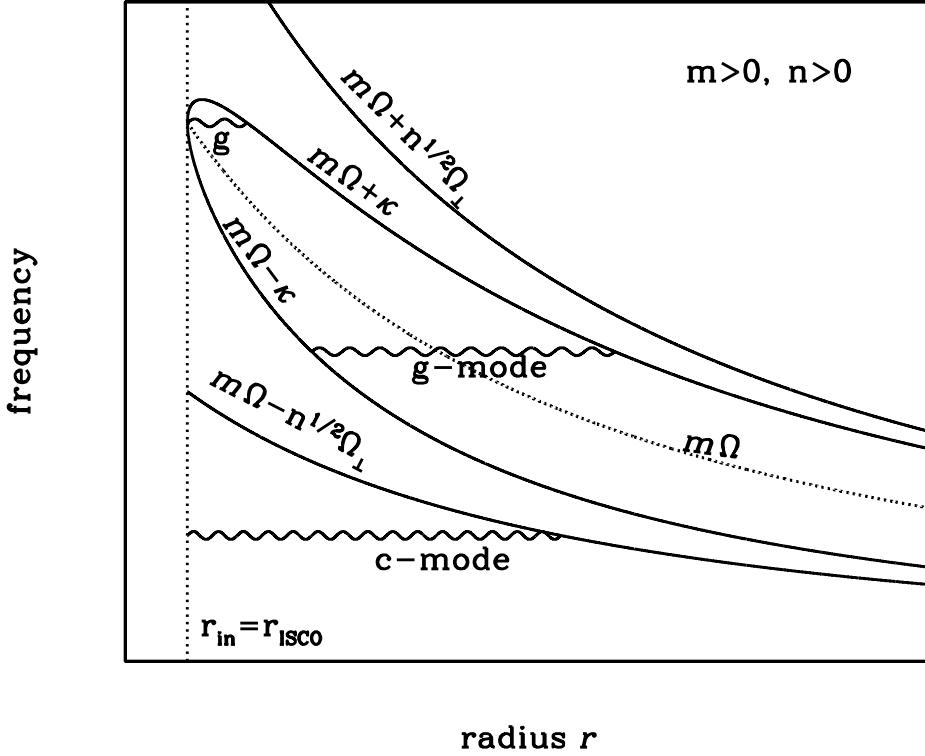


Figure 1. The propagation diagram for non-axisymmetric g-modes and c-modes. Note that the curves $m\Omega - \kappa$ and $m\Omega + \kappa$ meet at $r = r_{\text{ISCO}}$ since $\kappa(r_{\text{ISCO}}) = 0$ due to general relativistic effects. The g-modes are trapped between the inner Lindblad resonance (where $\omega = m\Omega - \kappa$) and the outer Lindblad resonance (where $\omega = m\Omega + \kappa$), or around the peak of the $m\Omega + \kappa$ curve.

3 PROPAGATION DIAGRAM AND C-MODES

There are three possible critical resonant points in the disc: the Lindblad resonances (LRs) where $D = 0$, the vertical resonances (VR) where $\tilde{\omega}^2 = n\Omega_\perp^2$, and the corotation resonance (CR) where $\tilde{\omega} = 0$. Far from these critical points, the WKB dispersion relation [for $\delta h \propto \exp(i \int k dr)$] takes the form (Okazaki et al. 1987)

$$c_s^2 k^2 = \frac{(\kappa^2 - \tilde{\omega}^2)(n\Omega_\perp^2 - \tilde{\omega}^2)}{\tilde{\omega}^2}. \quad (13)$$

The modes with $n = 0$ have no vertical structure, and are referred to as p-modes – their stability properties are studied in Lai & Tsang (2008). We focus on the modes with $n \geq 1$ and $m \geq 1$ in this paper. Wave propagation is allowed in regions where $\tilde{\omega}^2 < \kappa^2 < n\Omega_\perp^2$ or $\tilde{\omega}^2 > n\Omega_\perp^2 > \kappa^2$ (note that $\kappa < \Omega_\perp$ in GR). The former defines the g-mode propagation zone: the mode is trapped in the region where $m\Omega - \kappa < \omega < m\Omega + \kappa$; the latter leads to c-modes, for which the wave zone is specified by $\omega < m\Omega - \sqrt{n}\Omega_\perp$ (see Fig. 1). Clearly, the c-modes exist only when $m\Omega - \sqrt{n}\Omega_\perp > 0$ and wave reflection occurs at $r = r_{\text{in}} = r_{\text{ISCO}}$, the radius of the Inner-most Stable Circular Orbit. For Newtonian discs, since $\Omega_\perp = \kappa = \Omega$ the c-modes can only exist if $m > \sqrt{n}$; for relativistic discs, however, $\Omega > \Omega_\perp$ (for spinning black holes), we can obtain modes for $m = \sqrt{n}$ that may have very low frequencies. The “fundamental” c-mode, with $m = n = 1$ is of particular interest (Kato 1990), since it corresponds to the Lense-Thirring precession of the inner, tilted disc. Note that for extremely low mode frequencies, the terms of order $1/r$ previously ignored may become important, and care must be taken to obtain the real eigenfrequencies for trapped modes. Here we ignore these complications and refer to Silbergleit et al. (2001) for a more thorough relativistic analysis.

4 WAVE ABSORPTION AT THE COROTATION RESONANCE

The Lindblad resonances ($D = 0$) are apparent singularities of the master equation (9) [this can be seen easily by writing (9) as two coupled first-order differential equations], and no wave absorption occurs at the Lindblad resonances (e.g., Goldreich & Tremaine 1979; Li et al. 2003; Zhang & Lai 2006). The vertical resonances (where $\tilde{\omega}^2 = n\Omega_\perp^2$) act purely as turning points, and no wave absorption occurs there either. However, the corotation resonance must be treated more carefully (Kato 2003; Li et al. 2003; Zhang & Lai 2006).

Here we follow the analysis of Zhang & Lai (2006). Near the corotation ($r = r_c$, where $\omega = m\Omega$), equation (9) can be written as

$$\frac{d^2}{dr^2}\delta h - \frac{D(\tilde{\omega}^2 - n\Omega_\perp^2)}{c_s^2\tilde{\omega}^2}\delta h \simeq 0, \quad (14)$$

since for a thin disc the sound speed $c_s \ll r\Omega$ and the last term in (9) dominates the other terms. Defining $x \equiv (r - r_c)/r_c$ and expanding (14) around $x = 0$, we have

$$\frac{d^2}{dx^2}\delta h + \frac{C}{(x + i\epsilon)^2}\delta h = 0, \quad (15)$$

where

$$C \equiv \frac{n}{m^2} \left(\frac{\kappa\Omega_\perp}{c_s d\Omega/dr} \right)_{r_c}^2 \gg 1. \quad (16)$$

In equation (15), we have inserted a small imaginary part $i\epsilon$ (with $\epsilon > 0$) in $1/x^2$ because we consider the response of the disc to a slowly growing perturbation.

The two independent solutions to equation (15) are

$$\delta h_\pm = z^{1/2} z^{\pm i\nu} = z^{1/2} e^{\pm i\nu \ln z} \quad (17)$$

where $\nu = \sqrt{C - \frac{1}{4}} \gg 1$ and $z = x + i\epsilon$. The solution $z^{1/2} z^{i\nu}$ has a local wavenumber $k = d(\nu \ln z)/dr = \nu/(r_c x)$, with the group velocity $v_g = d\omega/dk = -\tilde{\omega}/k = -qr_c x^2 \omega/\nu < 0$ (where we have assumed $\Omega \propto r^{-q}$, with $q > 0$), thus it represents waves propagating toward small r . Similarly, the solution $z^{1/2} z^{-i\nu}$ has $v_g > 0$ and represents waves propagating toward large r .

As shown in Zhang & Lai (2006), waves with $n \geq 1$ can propagate into the corotation region and be absorbed there. Consider an incident wave propagating from the $x < 0$ (or $r < r_c$) region toward $x = 0$, with the amplitude (up to a constant factor)

$$\delta h(x < 0) = z^{1/2} e^{-i\nu \ln z} = i e^{\pi\nu} (-x)^{1/2} e^{-i\nu \ln(-x)}, \quad (\text{incident wave}). \quad (18)$$

The transmitted wave is simply

$$\delta h(x > 0) = x^{1/2} e^{-i\nu \ln x}, \quad (\text{transmitted wave}), \quad (19)$$

and there is no reflection. Thus the amplitude of the transmitted wave is decreased by a factor of $e^{-\pi\nu}$ (Zhang & Lai 2006). Similarly, a wave incident from the $r > r_c$ region toward r_c encounters the same attenuation. Since $\nu \gg 1$ for thin discs, We readily conclude that all waves incident upon the corotation will be absorbed (Kato 2003; Li et al. 2003; see Zhang & Lai 2006 and Lai & Zhang 2008 for applications of this result to the problem of wave excitation by external forces).

5 COROTATIONAL DAMPING OF C-MODES

The result of section 4 shows that waves propagating through the corotation are heavily damped. Since g-modes trapped between the inner and outer Lindblad resonances must cross the corotation, they are damped very quickly by corotation absorption, as shown by Kato (2003) and Li et al. (2003). Only higher frequency g-modes which are trapped around the peak of $m\Omega + \kappa$ (see Fig. 1) can avoid such corotational damping; these modes have frequencies $\omega \simeq m\Omega(r_{\text{ISCO}})$.

In this section we calculate the damping rate of the c-mode. The damping mechanism is illustrated in Fig. 2, where we also plot the effective potential:

$$V_{\text{eff}}(r) = \frac{D(\tilde{\omega}^2 - n\Omega_\perp^2)}{c_s^2\tilde{\omega}^2} + \frac{m^2}{r^2} + \frac{2m\Omega}{r\tilde{\omega}} \left(\frac{d}{dr} \ln \frac{\Omega\Sigma}{D} \right). \quad (20)$$

Based on the result of section 4, we will adopt the approximation that a wave transmitted through the barrier between the inner vertical resonance (IVR) and the inner Lindblad resonance (ILR) are absorbed at the corotation. We will also assume that the inner disc boundary is completely reflective (see section 6).

5.1 Reflection Coefficient

We first calculate the reflection coefficient \mathcal{R} when a wave in region I (see Fig. 2) propagates outward and is reflected back at the IVR.

From the dispersion relation (13), the group velocity of the wave is given by

$$v_g \equiv \frac{d\omega}{dk} = \frac{kc_s^2}{\tilde{\omega} \left[1 - (\kappa/\tilde{\omega})^2 (n\Omega_\perp^2/\tilde{\omega}^2) \right]}. \quad (21)$$

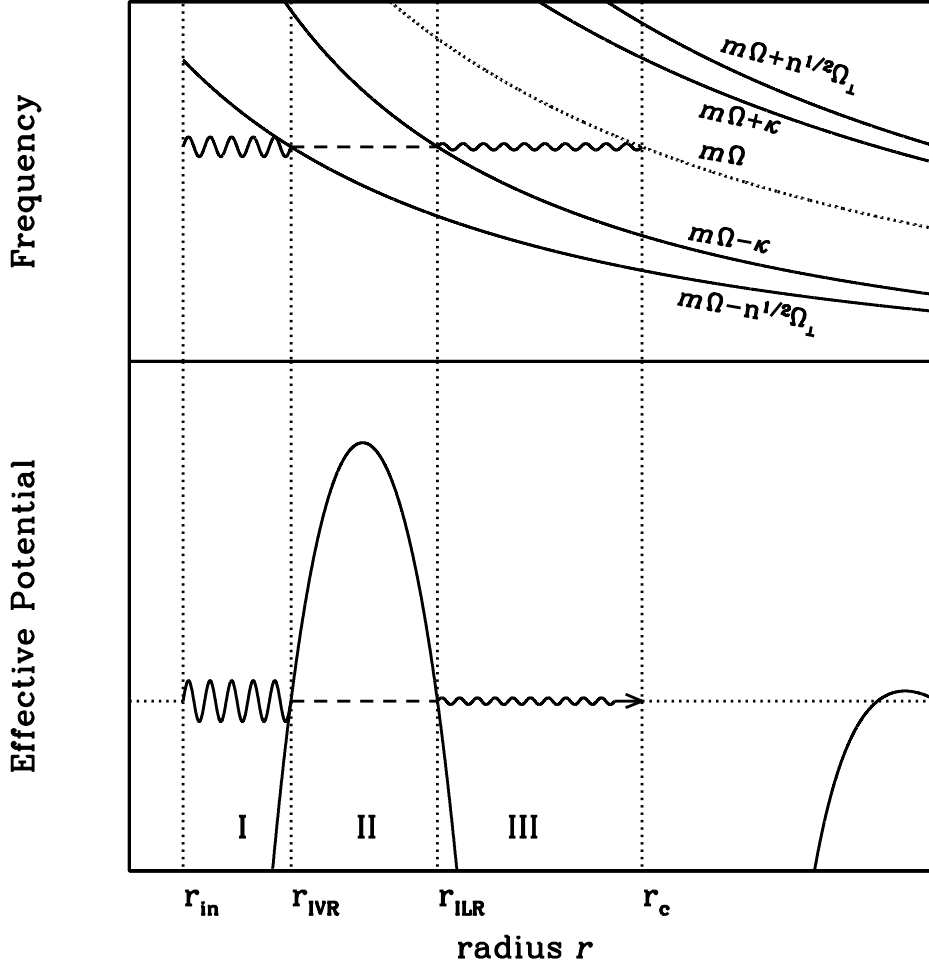


Figure 2. The wave propagation diagram (upper panel) and effective potential (lower panel) for c-modes. The modes are trapped in region I (between $r_{\text{in}} = r_{\text{ISCO}}$ and the inner vertical resonance r_{IVR}), but can tunnel through an evanescent barrier (region II, between the IVR and the inner Lindblad resonance r_{ILR}) and propagate into the corotation (r_c), where they are absorbed.

The relative sign of v_g and the phase velocity $v_p = \omega/k$ is important. In region III ($r_{\text{ILR}} < r < r_c$), v_g and v_p have the same sign, thus waves propagating outwards correspond to $k > 0$. In region I ($r < r_{\text{IVR}}$), v_g and v_p have opposite signs, so that waves propagating outwards have $k < 0$ and waves propagating inwards have $k > 0$.

As shown in the previous section we can, to good approximation, assume that waves propagating into the corotation are completely damped. Thus, only an outward-propagating wave exists in region III (see Fig. 2), with the wave amplitude (up to a constant prefactor) given by

$$\delta h = A \exp \left(i \int_{r_{\text{ILR}}}^r k dr + \frac{\pi}{4} \right), \quad (22)$$

where $k > 0$ is given by equation (13) and $A \equiv \sqrt{D/rk\Sigma}$ is the WKB amplitude. The connection formulae for the ILR (Tsang & Lai 2008) are

$$\delta h_1 \sim \begin{cases} \frac{1}{2} A \exp \left(- \int_r^{r_{\text{ILR}}} |k| dr \right) & \text{for } r \ll r_{\text{ILR}} \\ A \cos \left(\int_{r_{\text{ILR}}}^r k dr + \pi/4 \right) & \text{for } r \gg r_{\text{ILR}} \end{cases} \quad (23)$$

$$\delta h_2 \sim \begin{cases} A \exp \left(\int_r^{r_{\text{ILR}}} |k| dr \right) & \text{for } r \ll r_{\text{ILR}} \\ A \sin \left(\int_{r_{\text{ILR}}}^r k dr + \pi/4 \right) & \text{for } r \gg r_{\text{ILR}}. \end{cases} \quad (24)$$

These then give for the evanescent zone (region II in Fig. 2):

$$\delta h \simeq \frac{A}{2} \exp \left(- \int_r^{r_{\text{ILR}}} |k| dr \right) + i A \exp \left(\int_r^{r_{\text{ILR}}} |k| dr \right)$$

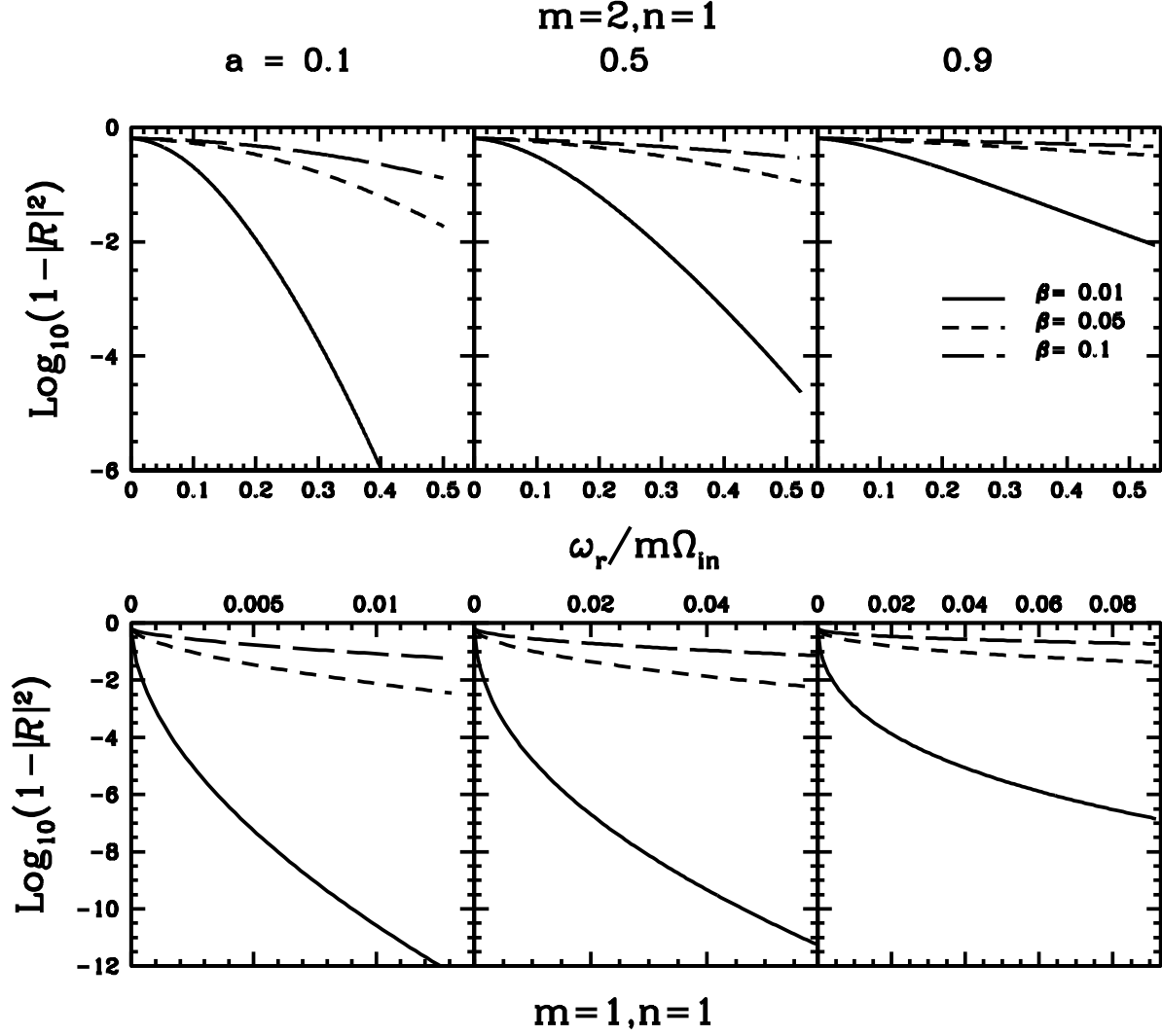


Figure 3. The reflection coefficient, \mathcal{R} , of waves incident upon the inner vertical resonance (IVR), as a function of the (real) wave frequency ω_r (in units of $m\Omega_{\text{in}}$, where Ω_{in} is the disc rotation rate at $r = r_{\text{in}}$), for various black hole spin parameters (a) and sound speeds $c_s = \beta r \Omega_{\text{in}}$. The upper panels are for $m = 2$, $n = 1$ and the lower panels for $m = n = 1$.

$$= \frac{A}{2} \exp(-\Theta_{\text{II}}) \exp\left(\int_{r_{\text{IVR}}}^r |k| dr\right) + iA \exp(+\Theta_{\text{II}}) \exp\left(-\int_{r_{\text{IVR}}}^r |k| dr\right) \quad (25)$$

where

$$\Theta_{\text{II}} = \int_{r_{\text{IVR}}}^{r_{\text{ILR}}} |k| dr. \quad (26)$$

The connection formulae at the IVR can be similarly derived; they are ¹

$$\delta h_1 \sim \begin{cases} \frac{1}{2} A \exp\left(-\int_{r_{\text{IVR}}}^r |k| dr\right) & \text{for } r \gg r_{\text{IVR}} \\ A \sin\left(\int_r^{r_{\text{IVR}}} k dr + \pi/4\right) & \text{for } r \ll r_{\text{IVR}} \end{cases} \quad (27)$$

$$\delta h_2 \sim \begin{cases} A \exp\left(\int_{r_{\text{IVR}}}^r |k| dr\right) & \text{for } r \gg r_{\text{IVR}} \\ A \cos\left(\int_r^{r_{\text{IVR}}} k dr + \pi/4\right) & \text{for } r \ll r_{\text{IVR}} \end{cases} \quad (28)$$

¹ Note that around the IVR, the differential equation is matched by the Airy functions, rather than by the Airy function derivatives as in the case of the ILR.

(Abramowitz & Stegun 1964). Thus, we find that for $r < r_{\text{IVR}}$ (region I in Fig. 2),

$$\delta h \simeq \frac{A}{2} e^{-\Theta_{\text{II}}} \cos \left(\int_r^{r_{\text{IVR}}} k dr + \frac{\pi}{4} \right) + i 2 A e^{\Theta_{\text{II}}} \sin \left(\int_r^{r_{\text{IVR}}} k dr + \frac{\pi}{4} \right). \quad (29)$$

Expressing this in terms of traveling waves and defining $y = \int_{r_{\text{IVR}}}^r k dr - \pi/4$, we have

$$\delta h \simeq i A \left[e^{-iy} \left(e^{+\Theta_{\text{II}}} + \frac{1}{4} e^{-\Theta_{\text{II}}} \right) - e^{+iy} \left(e^{\Theta_{\text{II}}} - \frac{1}{4} e^{-\Theta_{\text{II}}} \right) \right], \quad (30)$$

where the first term ($\propto e^{-iy}$) corresponds to the incident (outgoing) wave and the second term ($\propto e^{iy}$) the inward going wave reflected from the IVR. Thus the reflection coefficient is

$$\mathcal{R} = - \frac{e^{\Theta_{\text{II}}} - \frac{1}{4} e^{-\Theta_{\text{II}}}}{e^{\Theta_{\text{II}}} + \frac{1}{4} e^{-\Theta_{\text{II}}}}, \quad (31)$$

and the transmission coefficient (through region II) is

$$\mathcal{T} = \frac{i}{e^{\Theta_{\text{II}}} + \frac{1}{4} e^{-\Theta_{\text{II}}}}. \quad (32)$$

We can clearly see that $|\mathcal{R}|^2 < 1$.

5.2 Trapped C-modes and their Damping Rates

Assuming a reflective boundary exists at $r = r_{\text{in}} < r_{\text{IVR}}$, we can develop trapped c-modes in the inner disc, between r_{in} and the IVR. To illustrate this we consider a simple boundary condition at $r = r_{\text{in}}$:

$$\delta h(r_{\text{in}}) = 0. \quad (33)$$

From section 5.1, the wave in region I can be written as

$$\delta h = A \exp(-iy) + \mathcal{R} A \exp(iy), \quad \text{with } y = \int_{r_{\text{IVR}}}^r k dr - \pi/4. \quad (34)$$

where $k = k_r + i k_i$ is complex. Applying the boundary condition (33) to equation (34) yields the eigenvalue condition:

$$\exp(2i\Theta) = -i|\mathcal{R}|, \quad \text{with } \Theta = \int_{r_{\text{in}}}^{r_{\text{IVR}}} k dr = \Theta_r + i\Theta_i, \quad (35)$$

where Θ_r and Θ_i are real. The real eigen frequency ω_r is given by

$$\Theta_r = \int_{r_{\text{in}}}^{r_{\text{IVR}}} k_r dr = \int_{r_{\text{in}}}^{r_{\text{IVR}}} \frac{\sqrt{(\kappa^2 - \tilde{\omega}_r^2)(n\Omega_{\perp}^2 - \tilde{\omega}_r^2)}}{c_s |\tilde{\omega}_r|} dr = \mu\pi + \frac{3\pi}{4}, \quad (36)$$

where $\mu = 0, 1, 2, \dots$ is an integer and $\tilde{\omega}_r = \omega_r - m\Omega < 0$ in the trapping region between r_{in} and r_{IVR} . The imaginary part of the frequency ω_i is determined by $|\mathcal{R}| = \exp(-2\Theta_i)$, or

$$\tanh \Theta_i = - \left(\frac{|\mathcal{R}| - 1}{|\mathcal{R}| + 1} \right). \quad (37)$$

Note that $\Theta_i = \int_{r_{\text{in}}}^{r_{\text{IVR}}} k_i dr \ll 1$ and

$$k_i = \omega_i \frac{dk}{d\omega} \Big|_{\omega_r} = \frac{\omega_i \tilde{\omega}_r}{k_r c_s^2} \left(1 - \frac{n\kappa^2 \Omega_{\perp}^2}{\tilde{\omega}_r^4} \right). \quad (38)$$

We then obtain

$$\omega_i \simeq -\frac{1}{4} \exp(-2\Theta_{\text{II}}) \left[\int_{r_{\text{in}}}^{r_{\text{IVR}}} \frac{|\tilde{\omega}_r|^2}{\sqrt{(\kappa^2 - \tilde{\omega}^2)(n\Omega_{\perp}^2 - \tilde{\omega}^2)}} \left(1 - \frac{n\kappa^2 \Omega_{\perp}^2}{\tilde{\omega}_r^4} \right) \frac{dr}{c_s} \right]^{-1}. \quad (39)$$

Note that in the trapping region (between r_{in} and r_{IVR}), $n\kappa^2 \Omega_{\perp}^2 / \tilde{\omega}^4 < 1$. Thus the mode is always damped ($\omega_i < 0$).

5.3 Numerical Results

Figure 3 depicts the reflection coefficients for waves impinging upon the inner vertical resonance (IVR) from $r < r_{\text{IVR}}$ as a function of the wave frequency. We consider both the $m = 2, n = 1$ and the $m = 1, n = 1$ modes. The real frequency ranges from 0 to $(m\Omega - \sqrt{n}\Omega_{\perp})|_{r_{\text{in}}}$. Obviously, waves with higher frequencies are “protected” by a wider evanescent zone (see Figs. 1-2) and have $|\mathcal{R}|^2$ closer to unity.

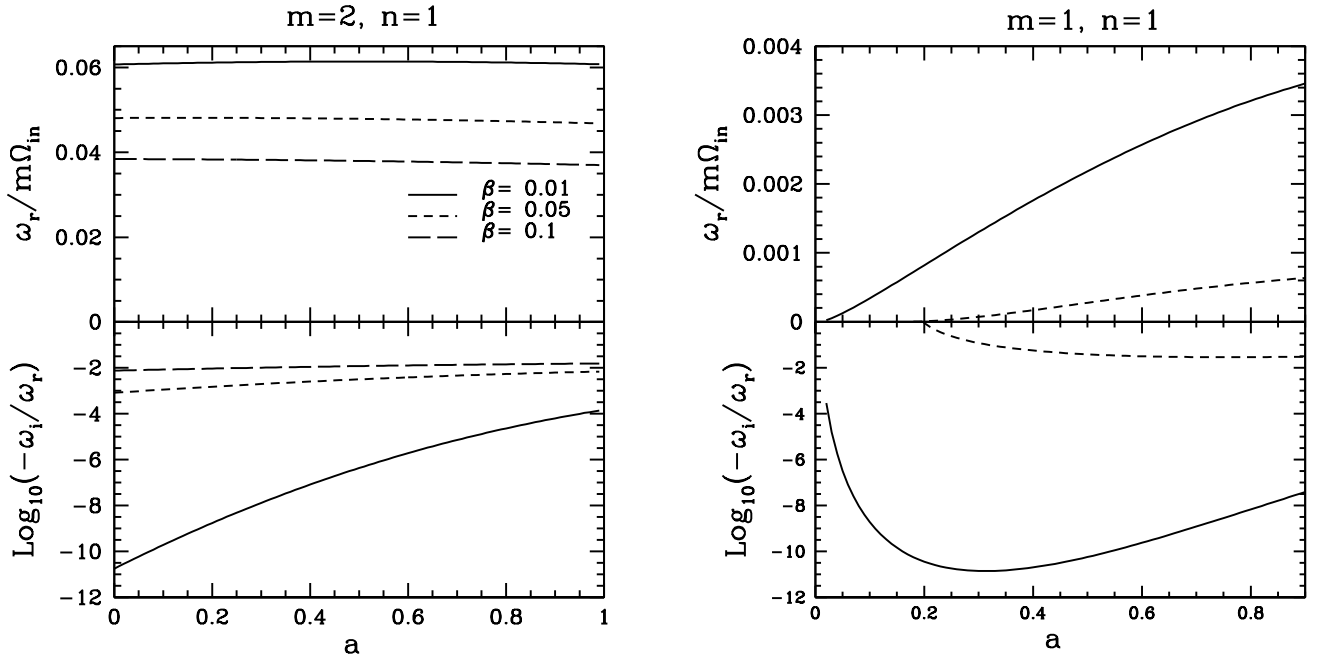


Figure 4. The real and imaginary frequencies for the primary trapped c-mode with the $\delta h(r_{\text{in}}) = 0$ boundary condition and $r_{\text{in}} = r_{\text{ISCO}}$ for various sound speeds versus the black hole spin parameter. Note that there is no mode for the one-armed corrugation wave (the right panel) for sound speed $c_s = 0.1r_{\text{in}}$.

Figures 4-5 show the real and imaginary c-mode frequencies, computed using the WKB expressions derived in section 5.2. Waves with higher frequencies have smaller damping rate $|\omega_i|$, consistent with the reflectivity results shown in Fig. 3. The damping rate is also smaller for cooler (smaller β) discs. Note that although we use the relativistic frequencies (10)-(12) our calculations not fully relativistic, and the real frequencies calculated shown in Fig. 4, particularly for the $m = n = 1$ mode with large black hole spin parameter a , are correct only in orders of magnitude [Fully relativistic calculation of the real frequencies of these trapped modes was done by Silbergleit et al. (2001).] Also note that adopting different inner disc boundary conditions would lead to different real mode eigenfrequencies than presented in Fig. 4.

Finally, we note that equation (39) is valid only when there is no loss of wave energy at the inner disc boundary r_{in} . In the presence of the rapid radial inflow at the ISCO, we would expect additional mode damping due to the leakage of waves into the plunging region of the disc (see Lai & Tsang 2008 for a study of such leakage for p-modes). Alternatively, a sufficiently strong excitation mechanism is needed to overcome the corotational damping and make the c-modes grow.

6 CONCLUSION

In this paper, we have shown that diskoseismic c-modes suffer corotational damping due to wave absorption at the corotation resonance. These modes are trapped between the inner disc edge and the inner vertical resonance (where $\omega - m\Omega = -\sqrt{n}\Omega_{\perp}$, with $m, n \geq 1$), but can tunnel through the evanescent zone and leak out to the corotation zone where wave absorption occurs. The mode damping rates are generally much smaller than the mode frequencies, and depend sensitively on the disc sound speed and the black hole spin parameters.

With this paper, we now have in hand a complete picture of how the corotation resonance affects various diskoseismic modes in black-hole accretion discs, at least in the linear regime: Non-axisymmetric g-modes are heavily damped at the corotation resonance (Kato 2003; Li et al. 2003), while p-modes (inertial-acoustic modes) can be overstable due to the corotational wave absorption (see Lai & Tsang 2008 and references therein). The corotational damping rates of c-modes are much smaller than those of g-modes.

Diskoseismic c-modes have been invoked to explain low-frequency variabilities in black-hole X-ray binaries (van der Klis 2006; Remillard & McClintock 2006). Fu & Lai (2008) showed that the basic properties of c-modes are largely unaffected by the disc magnetic fields and thus these modes are present in real discs. The results presented in this paper show that in order for the c-modes to be observable, a sufficiently strong excitation mechanism is needed to overcome the corotational damping.

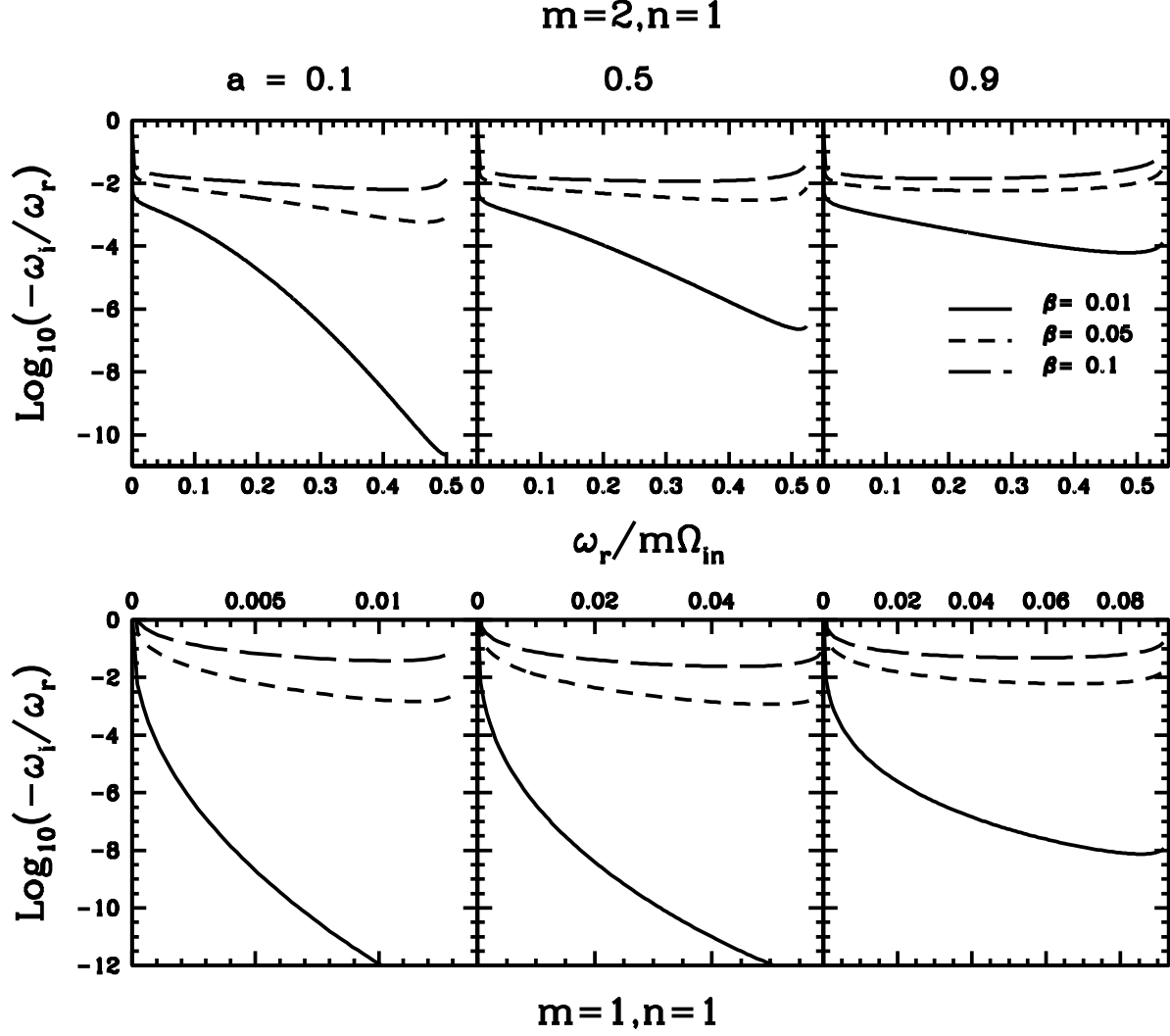


Figure 5. The damping rate $|\omega_i|$ for various sound speeds and black hole spin parameters for c-modes with purely reflective boundary conditions at r_{in} as a function of the real mode frequencies ω_r . The upper panels show the results for the $m = 2, n = 1$ modes and the lower panels show the $m = n = 1$ modes. The sound speeds are taken to be constant, $c_s = \beta r \Omega_{in}$.

ACKNOWLEDGMENTS

This work has been supported in part by NASA Grant NNX07AG81G, NSF grants AST 0707628, and by *Chandra* grant TM6-7004X (Smithsonian Astrophysical Observatory).

REFERENCES

- Abramowitz M. & Stegun I.A., 1964, Handbook of Mathematical Functions. Dover Press, New York
- Aliev, A.N., Gal'tsov, D.V. 1981, General Relativity and Gravitation, 13, 899
- Fu, W., Lai, D. 2008, ApJ, in press (arXiv:0806.1938)
- Goldreich, P., Tremaine, S. 1979, ApJ, 233, 857
- Ipser, J.R., 1994, ApJ, 435, 767
- Ipser, J.R., 1996, ApJ, 458, 508
- Kato, S. 1983, PASJ, 35, 249
- Kato, S., 1989, PASJ, 41, 745
- Kato, S., 1990, PASJ, 42, 99

- Kato, S., 2001, PASJ, 53, 1
Kato, S., 2003, PASJ, 55, 257
Kato, S. & Fukue, J., 1980, PASJ, 32, 377
Lai, D. & Tsang, D., 2008, MNRAS, submitted
Lai, D., Zhang, H. 2008, ApJ, 683, 949
Lee, W. H., Abramowicz, M. A. & Kluzniak, W., 2004, ApJ, 603, L93
Li, L. X., Goodman, J. & Narayan, R., 2003, ApJ, 593, 980
Nowak, M. A. & Wagoner, R. V., 1992, ApJ, 393, 697
Okazaki, A.T. & Kato, S., 1985, PASJ, 37, 683
Okazaki, A.T., Kato, S., & Fukue, J., 1987, PASJ, 39, 457
Perez, C.A., Silbergleit, A.S., Wagoner, R.V. & Lehr, D.E., 1997, ApJ, 476, 589
Paczynski, B. & Wiita, P.J. 1980, A&A 88, 23
Remillard, R. A. & McClintock, J. E., 2006, ARAA, Vol. 44, pp. 49-92
Silbergleit, A. S., Wagoner, R. V. & Ortega-Rodriguez, M., 2001, ApJ, 548, 335
Tsang, D. & Lai, D., 2008, MNRAS, 387, 446
van der Klis, M. 2006, in Compact Stellar X-ray Sources, ed. W.H.G. Lewin and M. van der Klis (Cambridge Univ. Press) (astro-ph/0410551)
Wagoner, R. V., 1999, Phys. Rep., 311, 259
Zhang, H. & Lai, D., 2006, MNRAS, 368, 917